Electronic Supplementary Information (ESI) for Chemical Communications

This journal is (c) The Royal Society of Chemistry 2013

In situ generated AgBr-enhanced ZnO nanorod-based photoelectrochemical aptasensing via layer-by-layer assembly

Jing Li,[†, ‡] *Wenwen Tu,*[†] *Hongbo Li,*[*, ‡] *Jianchun Bao,*[†] *Zhihui Dai,*[*, †]

[†]Jiangsu Key Laboratory of Biofunctional Materials, College of Chemistry and Materials Science, Nanjing Normal University, Nanjing 210023, P.R. China

[‡]College of Chemical and Biological Engineering, Yancheng Institute of Technology, Yancheng 224051, P.R. China

E-mail: daizhihuii@njnu.edu.cn, hbli@ycit.edu.cn

Contents:

Experimental Section

Materials and Reagents. Indium tin oxide (resistivity 10 Ω/sq.) is obtained from Zhuhai Kaivo Electronic Components Co. Ltd., China. $Zn (NO_3)_2{\cdot}6H_2O$ (≥ 99.0%), Mercury (II) chloride ($HgCl_2$), Poly dimethyl diallyl ammonium chloride (PDDA; 20 wt% in water, M_w (200,000-350,000)) and tris-(hydroxymethyl)-aminomethane were bought from Sigma-Aldrich (St. Louis, MO). KNO_3, $AgNO_3$, NaBr and other chemicals were purchased from Sinopharm Chemical Co., Ltd. (Shanghai, China). Oligonucleotides were obtained from Sangon Biotechnology Co., Ltd. (Shanghai, China) and had the sequences as: 5’-CCC CCC CCC CCC CCC CCC-3’ (poly (C)). The stock solution of poly (C) was 100 μmol L^{-1} in 10 mmol L^{-1} TE buffer solution (pH 8.0) and kept frozen. 10 mmol L^{-1} Tris-HCl (pH 7.4) was used to dilute the stock solution when needed. The stock solution of Ag^+ was prepared from $AgNO_3$ with the concentration of 1 mmol L^{-1}. In this work, 0.1 mol L^{-1} phosphate-buffered saline (PBS) was always employed as the supporting electrolyte and the pH value of PBS was 7.0 unless indicated otherwise. Millipore ultrapure water (resistivity ≥ 18.2 MΩ·cm) was used throughout the experiment and all chemicals were of analytical reagent grade. AgBr was obtained in the characterizations of UV-vis spectroscopy and XRD as following: Equal volume of 10 mmol L^{-1} $AgNO_3$ and 0.1 mol L^{-1} NaBr solutions were mixed and shaken for a few minutes, and then a yellow precipitate emerged. The above mixture was further shaken to get a homogeneous emulsion, and then 100 uL of the emulsion was dropped onto the ITO electrode (1 cm × 1 cm) and dried at room temperature in the dark.

Apparatus. Digital Lux Meter (MS6612, Shenzhen Huayi Instrument Co. Ltd., China). Field Emission Scanning Electron Microscopy (FESEM) and Energy dispersive spectrum (EDS) were performed with a JSM-5610LV/VANTAGE Ⅳ (JEOL, Japan and Thermo Electron, USA). X-ray diffraction (XRD) patterns of ZnO nanorods, AgBr and the composite film of ZnO-PDDA-poly (C)-AgBr (shortened as ZnO-AgBr) on ITO electrode (1 cm × 1 cm) were measured on the D/max 2500VL/PC diffractometer (RIGAKU, Japan) equipped with graphite monochromatized Cu Kα radiation (λ = 1.54056 Å) in 2θ ranging from 20° to 80° with a scan rate of 1.2° min^{-1} at 40 kV and 100 mA, respectively. UV-visible diffuse reflectance spectra were carried out in a quartz cuvette on a Cary 5000 UV-Vis-NIR spectrophotometer (Varian, USA). The controlled experiment for Ag^+ was performed using an Agilent 7500a ICP-MS (PaloAlto, CA, USA). PEC measurements were performed with a home-built PEC system. Photocurrent was measured by the current–time curve experimental technique on a CHI660D electrochemical workstation (CH Instruments, Shanghai, China) at a bias voltage of 0.2 V following a 250 W tungsten halogen light excitation. The distance between the light source and the electrode was fixed at 10 cm. All experiments were carried out at room temperature in the dark using a conventional three electrode system with a modified ITO (5.0 mm in diameter) as the working electrode, a platinum wire as the auxiliary electrode, and a standard Ag/AgCl in 3 mol L^{-1} KCl as the reference electrode. The error bars in the respective calibration curves were derived from a set of N=3 experiments.

Sensor Preparation and Detection Procedure. ZnO nanorod array was facilely prepared by electrodeposition according to the reference with some modifications.[S1] In detail, before electrodeposition, an ITO electrode (1 cm × 4 cm) was cleaned with NaOH (1 mol L^{-1}) and H_2O_2 (30%), washed with acetone and ultrapure water, respectively. The ZnO nanorods were electrodeposited for 2 h at 80 ^{o}C and -1.0 V vs a Ag/AgCl electrode in 3 mol L^{-1} KCl from a hybrid solution of 0.5 mmol L^{-1} $Zn(NO_3)_2 \cdot 6H_2O$ and 0.1 mol L^{-1} KNO_3 on ITO substrates (1 cm × 1 cm) in a three-electrode system. And then, the ZnO nanorods modified ITO electrodes were annealed to ensure particles adhesion to the substrate at 110 ^{o}C for 1 h in air. Next, 10 μL of 2.0 % PDDA containing 0.5 mol L^{-1} KNO_3 was dropped onto the ZnO nanorod array modified ITO electrode for 10 min. Following, 10 μL of 10 μmol L^{-1} poly (C) was assembled onto the modified electrode for 20 min via electrostatic interaction. After each step in the above assembly, the modified ITO electrode was washed with ultrapure water, and dried at room temperature. And thus, Ag^+ was selectively detected according to the C-Ag^+-C coordination chemistry[S2] and then in situ generated AgBr-enhanced ZnO nanorod-based photocurrent. Typically, 10 μL of $AgNO_3$ solution was dropped onto the modified electrode for 30 min, followed by thoroughly rinsing with ultrapure water and dried at room temperature in the dark. Finally, 10 μL of 0. 1 mol L^{-1} NaBr solution was dropped and incubated for 30 min at room temperature in the dark. After rinsed with copious water, the fabricated PEC sensor was applied to detect Ag^+ in 0.1 mol L^{-1} PBS (pH 7.0) by current–time curve experimental technique at the bias voltage of 0.2 V following the 250 W tungsten halogen light excitation. The controlled experiments were operated according to the same procedure except for the metal ions were other ones (Li^+, Na^+, K^+, Ca^{2+}, Mg^{2+}, Hg^{2+}, Zn^{2+}, Pb^{2+}, Cd^{2+} and Cu^{2+}) and common anions (F^-, Cl^-, Br^-, I^-, SO_4^{2-}, PO_4^{3-}, CO_3^{2-}). All the analyte concentrations mentioned in this work referred to the final concentration in the detected samples. Except the characterization, the annealed ZnO nanorods modified ITO electrode was masked off with an effective working area of a circle that had a diameter of 5 mm for further assembly and experiment.

Characterization of the ZnO Nanorod Array and the Modified Electrode. Fig. S1 showed the top view observations of ZnO nanorod array and the composite film of ZnO-PDDA-poly (C)-AgBr (ZnO-AgBr). The inset in Fig. S1A showed the top view of the ZnO nanorod array in a large magnification. As could be seen clearly in KCl from a hybrid solution of 0.5 mmol L^{-1} $Zn(NO_3)_2 \cdot 6H_2O$ and 0.1 mol L^{-1} KNO_3. And the synthesis yielded ZnO nanorods with diameters of 200-300 nm and lengths of 0.5-1.0 μm. It could be indexed to wurtzite structure of hexagonal ZnO, indicating its growth direction along [0001].[S3,S4] Fig. S1B showed the top view of ZnO-AgBr. It showed that a thin polymer film covered most of the ZnO nanorods, especially for those not vertical to the substrate. AgBr in the composite could not be seen in (B) owing to its very small size and the little quantity. But the mapping results based on the EDS pattern indicated that the composite film concluded Zn (C), O (D), Ag (E) and Br (F) (N, Cl and C not shown here). Quantitative analysis showed that mean atomic ratio of Zn/O in the ZnO nanorods is nearly stoichiometric. But the quantity of Br (F) was obviously more than that of Ag (E). This is owing to the much excess

NaBr used in the assembly and the insufficient washing in the last step. However, the excess NaBr did no harm to the detection, actually it helped to enhance the photocurrent by digesting the holes left like that in photocatalysis.[S5] In summary, these data confirmed the high purity of the ZnO-nanorod and the successful assembly of ZnO-AgBr.

Fig. S2 showed the XRD patterns of (a) ZnO, (b) ZnO-AgBr, (c) AgBr. All the peaks showed the existence of ZnO (JCPDS card No.36-1451) and AgBr (JCPDS card No.06-0438), respectively. And it could be suitably indexed to wurtzite (hexagonal) zinc oxide with a lattice constant of a=b=3.249 Å and c=5.206 Å, which agreed well with the FESEM (inset in Fig. S1A) and also the JCPDS. The phase of AgBr was cubic, and the lattice constant of a=b=c=5.774 Å was in agreement with the literature.[S6] No peaks for other impurities were found in the spectra, revealing the high purity of both products. The sharp and narrow peaks indicated that the nanostructures were highly crystallized. As expected, a substantially higher intensity was observed for the (002) diffraction peak in the XRD patterns of the ZnO nanorod arrays (a), indicating that the ZnO nanorods were highly oriented with their c-axes being perpendicular to the ITO glass substrate,[S3] which was well consistent with the FESEM result in Fig. S1A.

The UV-vis diffuse reflectance spectra of ZnO (black), ZnO-AgBr (red), and AgBr (green) are presented in Fig. S3. Although the reflectance was observed in the whole visible wavelength range, the most pronounced enhancement occurred at 395 nm, corresponding to the optical bandgap of about 3.2 eV. This agreed well with the literatures under similar deposition conditions.[S4] Compared with the ZnO single crystal which has the optical band gap of 3.37 eV and the band edge of 376 nm,[S7] the band edge here was a little red shift. The red shift band edge and the reflectance in the whole visible region were due to the larger diameter of ZnO nanorods and the more strong light scattering effect here.[S8] This scattering effect enhanced absorption due to long optical path-lengths and photonic effects which could persist in periodic vertically-oriented nanorod arrays.[S9] It also helped enhancing the photocurrent through multiple absorption. AgBr had a wide absorption peak in the region of 400-500 nm, which accorded well with the literatures.[S5,S10] Consequently, ZnO-AgBr exhibited a higher extinction intensity in the visible region than ZnO, which was beneficial for enhancing the photoresponse. Herein, both the light scattering effect of ZnO nanorod array and the AgBr sensitization helped the enhancement of the total light absorption for the modified electrode in the visible light region.

Optimization of Detection Conditions. The incubation time of Ag^+ and Br^- were important influencing factors for the sensitivity of the PEC sensing. Fig. S4A and S4B showed the incubation time effect of $AgNO_3$ and NaBr on the PEC sensing, respectively. As shown in Fig. S4A, after 30 min incubation of Ag^+, the photocurrent response arrived at a plateau. The incubation of largely excess Br^- is the same case as Ag^+ (Fig. S4B). Consequently, the incubation time for both Br^- and Ag^+ was selected as 30 min. In addition, pH effect on the response of the sensing system to Ag^+ was also evaluated as shown in Fig. S5. In the effective phosphate-buffered range of the pH value of 5.3-8.04, pH value has no significant effect on the sensing system to Ag^+. This result can be explained as follows: Firstly, there is no proton taking part in the reaction in the present sensing system. Secondly, as a kind of amphoteric compound, ZnO is relative inert in the presence of weak acid or base. Thirdly, PDDA can help keeping the stability of the ZnO in the presence of weak acid or base. Considering the pH of real samples, pH 7.0 was chosen for the experiments.

Table S1. The Comparison of Different Silver (I) Assay Methods

Method	Materials	DLR[a]	LOD[a]	Ref.
Colorimetric[d5]	Hemin/G-quadruplex DNAzyme	5-100 nM[b]	2.5 nM[d3]	S11
Colorimetric	Au NP-Citrate-Tween 20	400-1000 nM	100 nM[d3]	S12
UV-vis	Au nanorod	1 nM-100 μM[b]	10 nM[d4]	S13
Fluorescence	Al_2O_3 NP @Au nanodot	3-300 nM	1.5 nM[d4]	S14
Fluorescence	Graphene quantum dot	0-100 nM	3.5 nM[d2]	S15
Fluorescence	fluorophore probe	0.1-5.0 μM	0.13 μM[d1]	S16
Fluorescence[d5]	the pyrrolo-dC mismatched ds-DNA	0-100 nM	9.2 nM[d2]	S17
Fluorescence[d5]	CdSe/ZnS QD-labeled DNA	/	1 μM[d4]	S18
Fluorescence[d5]	SYER Green 1 as the DNA intercalator	50-700 nM	32 nM[d1]	S19
Fluorescence[d5]	FAM-labeled DNA-SWCNT	0-150 nM	1 nM[d2]	S20
Fluorescence[d5]	FAM-labeled DNA-GO	/	5 nM[d1]	S21
Fluorescence[d5]	$Ru(bpy)_2dppz^{2+}$-DNA-CdTe QDs	2 μM-10 μM	0.1 μM	S22
Fluorescence	Fluorophore Probe	/	10.2 nM	S23
Fluorescence[d5]	FAM-labeled DNA-nano C_{60}	/	1 nM	S24
CC[c,d5]	Au NPs and Cleavage NEase	1 pM[b]-100 nM	0.47 pM[d1]	S25
ISE[c]	Ionophore-doped sensing membranes	0.1-1 nM	38 pM[d4]	S26
PEC[c,d5]	ZnO nanorod array-PDDA-poly (C)-AgBr	0.4-12.8 nM	150 pM[d2]	This work

a DLR means dynamic linear range. LOD means limit of detection.

b nM means nmol L^{-1}, μM means μmol L^{-1}, pM means pmol L^{-1}.

c CC means chronocoulometry. ISE means ion-selective electrode. PEC means photoelectrochemical.

d1 LOD was defined at 3S/N.

d2 LOD was defined at 3σ/slope.

d3 LOD was defined as the lowest value that could be detected.

d4 LOD was not told.

d5 Aptamer-based sensor for Ag^+.

Interference and Application in Real Samples. The selectivity of this system for Ag^+ at 7.5 nmol L^{-1} was evaluated over other common metal ions and anions such as 1000-fold K^+, Na^+, Li^+, F^-, Cl^-, SO_4^{2-}, PO_4^{3-}, CO_3^{2-}; 200-fold Ca^{2+}, Mg^{2+}; 150-fold Br^-; 30-fold I^-; 20-fold Cu^{2+}, Cd^{2+}, Zn^{2+} and 10-fold Pb^{2+}, Hg^{2+}. As shown in Fig. S6A, only the solution containing Ag^+ was obviously "Signal On", whereas the others remained nearly unchanged (the deviation <5.0%). Neither Hg^{2+} nor Pb^{2+} disturbed Ag^+ detection, which was different from other detection methods.[S12-14,S18] This remarkably high selectivity was better than or at least comparable to other aptamer-based or the fluorescent iodide-based silver ion detection methods,[S11,S16-S21] let alone those nanomaterial-based methods.[S12-S15] This can be explained by both the highly specific interaction of C–Ag^+–C coordination effect[S2] and the specific ionic interaction between Ag^+ and Br^-, which is similar to that of Ag^+ and iodide.[S16] Moreover, the in situ generated AgBr could largely enhance the photocurrent by photosensitization. The dual function of AgBr here helps improving the analytical performances to a large extent. Additionally, the influences of common anions on Ag^+ assay were also performed. The results (Fig. S6B) showed that 1000-fold F^-, Cl^-, SO_4^{2-}, PO_4^{3-}, CO_3^{2-}; 150-fold Br^- and 30-fold I^- could coexit with Ag^+. Except for F^-, the concentration of any anion above is less than the critical value according to its corresponding K_{sp} constant value and the known concentration of Ag^+ added. Therefore, their influences on the capture and detection of Ag^+ could be ignored. The selectivity and real sample detection have confirmed this phenomena. This result could be explained by their difficulty to assembly onto the anion oligonucleotides owing to the electrostatic interaction and particularly the lack of specificity with poly (C).

On the bases of the above results, in order to evaluate the feasibility of the novel PEC sensor, we further challenged the performance of the sensor in real samples, i.e. the localized lake water by a standard addition method. After a minor pretreatment, consisting of successive filtration through Whatman filter No.1 and Minisart (0.45 μm), the real samples (5 mL) were added with 20 uL of 1 μmol L^{-1} $AgNO_3$. And then 10 uL of the mixed solution was dropped onto the modified ITO electrode prior to thoroughly rinsing with water and then incubated with 0.1 mol L^{-1} NaBr for 30 min before the PEC detection. The average recovery values were 95.0% and 107.4% (N=5) obtained by the PEC sensor and ICP-MS, respectively, indicating the potential practicality of the PEC sensor for environmental samples with little interferences. Additionally, this assay was inert toward the blank sample, suggesting the interference of materials in lake water, such as bacteria and pathogenic, can not be captured by the electrode and have little disturbance on the Ag^+ assay.

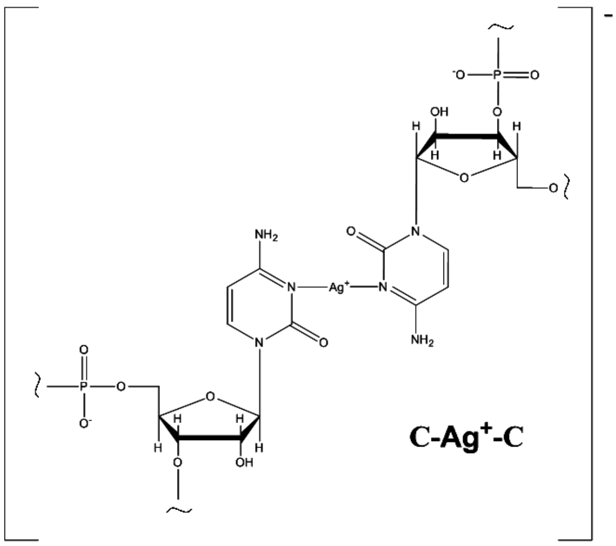

Scheme S1. The structure segments of C-Ag$^+$-C for Ag$^+$-mediated DNA molecular wire.

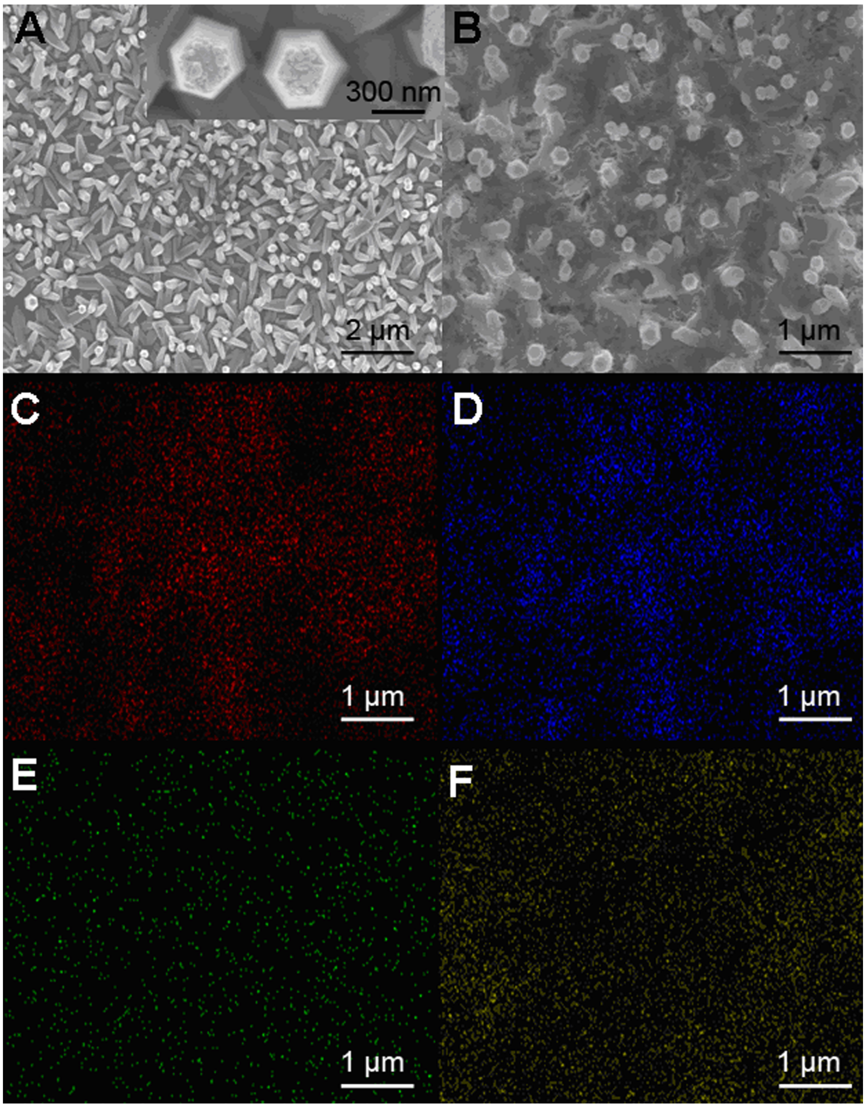

Fig. S1. FESEM images of (A) ZnO nanorod array, (B) ZnO-AgBr, Mapping of (C) Zn, (D) O, (E) Ag, (F) Br in the ZnO-AgBr composite film. The inset in (A) showed the top view of ZnO nanorod arrays in a large magnification.

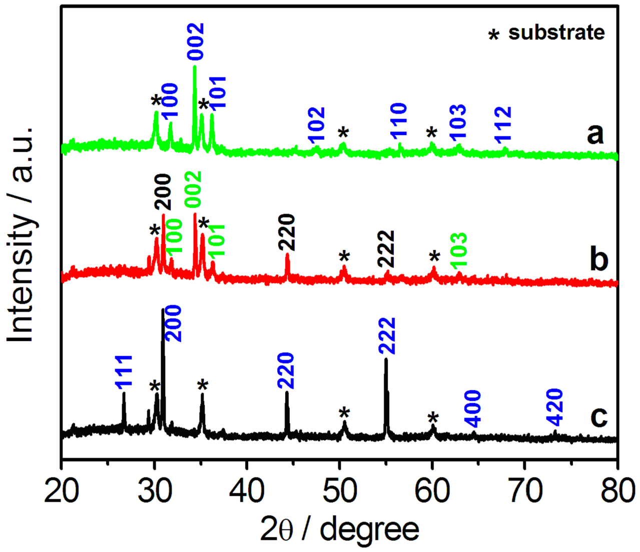

Fig. S2. The XRD patterns of (a) ZnO, (b) ZnO-AgBr, (c) AgBr

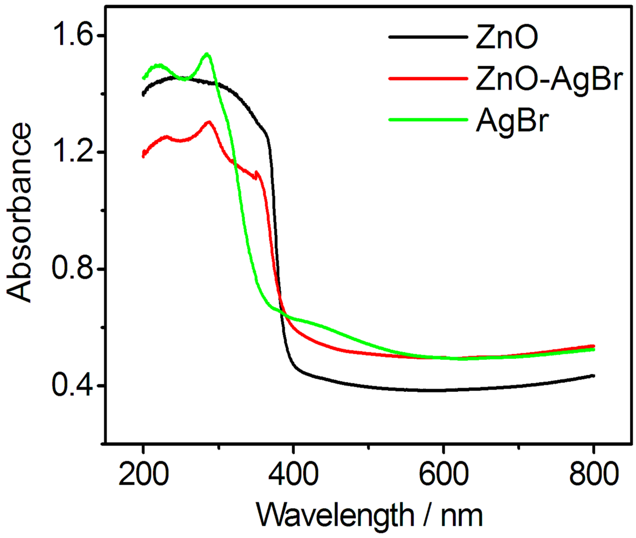

Fig. S3. UV-vis diffuse reflectance spectra of ZnO (black), ZnO-AgBr (red), and AgBr (green).

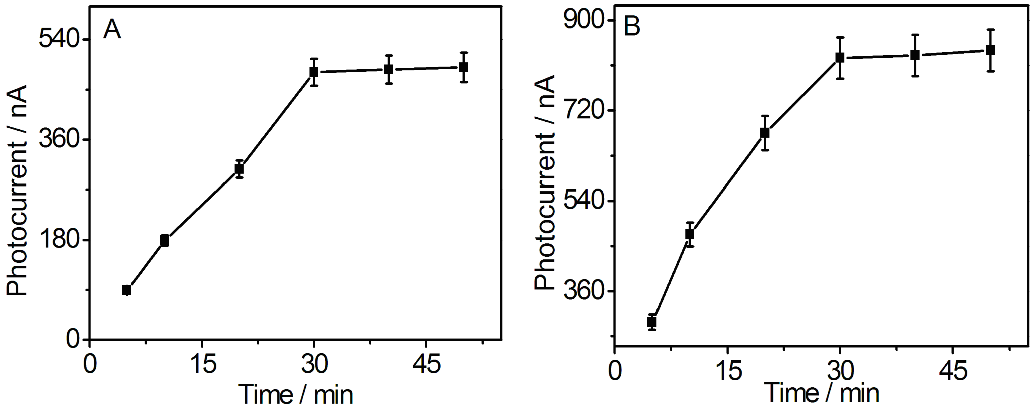

Fig. S4. Effects of the incubation time for (A) 7.5 nmol L^{-1} Ag^+ and (B) 0.1 mol L^{-1} Br^- on the response of the modified ITO electrodes in 0.1 mol L^{-1} PBS (pH 7.0) at the bias voltage of 0.2 V following the 250 W tungsten halogen light irradiation.

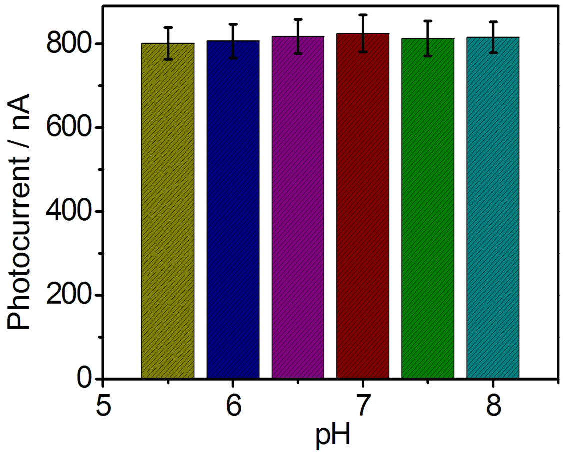

Fig. S5. The pH effects on the photocurrent responses of the ZnO-PDDA-poly (C)-AgBr modified ITO electrodes in 0.1 mol L^{-1} PBS in the presence of 7.5 nmol L^{-1} silver ions at the bias voltage of 0.2 V and following the 250 W tungsten halogen light (simulated sunlight) irradiation.

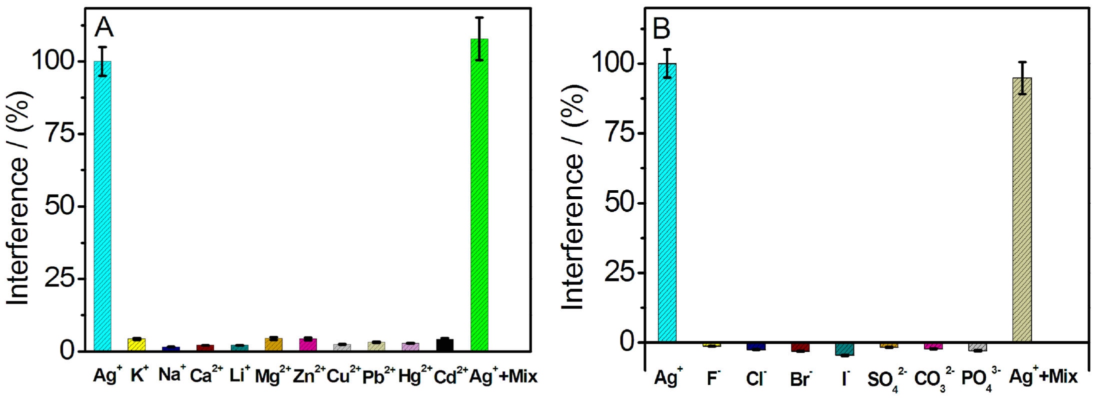

Fig. S6. Effects of common metal ions and anions on the detection of 7.5 nmol L^{-1} Ag^+ in 0.1 mol L^{-1} PBS (pH 7.0) at the bias voltage of 0.2 V following the 250 W tungsten halogen irradiation. The bars represent 7.5 nmol L^{-1} Ag^+ and a mixture of 7.5 nmol L^{-1} Ag^+ with one-tenth of the concentration of other ions mentioned as following: 1000-fold K^+, Na^+, Li^+, F^-, Cl^-, SO_4^{2-}, PO_4^{3-}, CO_3^{2-}; 200-fold Ca^{2+}, Mg^{2+}; 150-fold Br^-; 30-fold I^-; 20-fold Cu^{2+}, Cd^{2+}, Zn^{2+} and 10-fold Pb^{2+}, Hg^{2+}. Error bars represent the standard deviation of three replicates.

Supplementary References

[S1] J. F. Qiu, M. Guo, Y. J. Feng and X. D. Wang, *Electrochim. Acta,* 2011, **56**, 5776.

[S2] A. Ono, S. Cao, H. Togashi, M. Tashiro, T. Fujimoto, T. Machinami, S. Oda, Y. Miyake, I. Okamoto and Y. Tanaka, *Chem. Commun.,* 2008, 4825.

[S3] L. E. Greene, M. Law, J. Goldberger, F. Kim, J. C. Johnson, Y. F. Zhang, R. J. Saykally and P. D. Yang, *Angew. Chem. Int. Ed.,* 2003, **42**, 3031.

[S4] F. Xu, Y. Lu, Y. Xie and Y. Liu, *J. Solid State Electrochem.,* 2010, **14**, 63.

[S5] P. Wang, B. Huang, X. Zhang, X. Qin, H. Jin, Y. Dai, Z. Wang, J. Wei, J. Zhan, S. Wang, J. Wang and M. H. Whangbo, *Chem. Eur. J.,* 2009, **15**, 1821.

[S6] Q. Zhu, W. S. Wang, L. Lin, G. Q. Gao, H. L. Guo, H. Du and A. W. Xu, *J. Phys. Chem. C,* 2013, **117**, 5894.

[S7] W. I. Park, Y. H. Jun, S. W. Jung and Y. Gyu-Chul, *Appl. Phys. Lett.*, 2003, **82**, 964.

[S8] R. Tena-Zaera, J. Elias and C. Levy-Clement, *Appl. Phys. Lett.*, 2008, **93**, 233119.

[S9] (*a*) M. D. Kelzenberg, S. W. Boettcher, J. A. Petykiewicz, D. B. Turner-Evans, M. C. Putnam, E. L. Warren, J. M. Spurgeon, R. M. Briggs, N. S. Lewis and H. A. Atwater, *Nat. Mater*., 2010, **9**, 239; (*b*) M. Law, L. E. Greene, J. C. Johnson, R. Saykally and P. D. Yang, *Nat. Mater*., 2005, **4**, 455.

[S10] (*a*) P. Wang, B. B. Huang, X. Y. Qin, X. Y. Zhang, Y. Dai and M. H. Whangbo, *Inorg. Chem.,* 2009, **48**, 10697; (*b*) L. Q. Ye, J. Y. Liu, C. Q. Gong, L. H. Tian, T. Y. Peng and L. Zan, *ACS Catal.,* 2012, **2**, 1677.

[S11] T. Li, L. L. Shi, E. K. Wang and S. J. Dong, *Chem. Eur. J.,* 2009, **15**, 3347.

[S12] C. Y. Lin, C. J. Yu, Y. H. Lin and W. L. Tseng, *Anal. Chem.,* 2010, **82**, 6830.

[S13] H. W. Huang, S. N. Chen, F. Liu, Q. Zhao, B. Liao, S. J. Yi and Y. L. Zeng, *Anal. Chem.,* 2013, **85**, 2312.

[S14] P. C. Chen, T. Y. Yeh, C. M. Ou, C. C. Shih and H. T. Chang, *Nanoscale,* 2013, **5**, 4691.

[S15] X. Ran, H. J. Sun, F. Pu, J. S. Ren and X. G. Qu, *Chem. Commun.,* 2013, **49**, 1079.

[S16] A. Chatterjee, M. Santra, N. Won, S. Kim, J. K. Kim, S. B. Kim and K. H. Ahn, *J. Am. Chem. Soc.,* 2009, **131**, 2040.

[S17] K. S. Park, J. Y. Lee and H. G. Park, *Chem. Commun.,* 2012, **48**, 4549.

[S18] R. Freeman, T. Finder and I. Willner, *Angew. Chem. Int. Ed.,* 2009, **48**, 7818.

[S19] Y. H. Lin and W. L. Tseng, *Chem. Commun.,* 2009, 6619.

[S20] C. Zhao, K. G. Qu, Y. J. Song, C. Xu, J. S. Ren and X. G. Qu, *Chem. Eur. J.,* 2010, **16**, 8147.

[S21] Y. Q. Wen, F. F. Xing, S. J. He, S. P. Song, L. H. Wang, Y. T. Long, D. Li and C. H. Fan, *Chem. Commun.,* 2010, **46**, 2596.

[S22] W. Sun, J. Yao, T. Yao and S. Shi, *Analyst*, 2013, **138**, 421.

[S23] J. Hatai, S. Pal and S. Bandyopadhyay, *RSC Advances*, 2012, **2**, 10941.

[S24] H. Li, J. Zhai and X. Sun, *Analyst*, 2011, **136**, 2040.

[S25] P. Miao, L. Ning and X. Li, *Anal. Chem.,* 2013, **85**, 7966.

[S26] C. Z. Lai, M. A. Fierke, R. C. da Costa, J. A. Gladysz, A. Stein and P.

1 Bühlmann, *Anal. Chem.,* 2010, **82**, 7634.